The Astrophysical Journal, 842:1 (14pp), 2017 June 10 https://doi.org/10.3847/1538-4357/aa72ef

On the Origin of Sub-subgiant Stars. III. Formation Frequencies

Aaron M. Geller[1,2,6], Emily M. Leiner[3], Sourav Chatterjee[1], Nathan W. C. Leigh[4], Robert D. Mathieu[3], and Alison Sills[5]
[1] Center for Interdisciplinary Exploration and Research in Astrophysics (CIERA) and Department of Physics and Astronomy, Northwestern University, 2145 Sheridan Road, Evanston, IL 60201, USA; a-geller@northwestern.edu
[2] Adler Planetarium, Department of Astronomy, 1300 S. Lake Shore Drive, Chicago, IL 60605, USA
[3] Department of Astronomy, University of Wisconsin-Madison, 475 North Charter Street, Madison, WI 53706, USA
[4] Department of Astrophysics, American Museum of Natural History, Central Park West and 79th Street, New York, NY 10024, USA
[5] Department of Physics and Astronomy, McMaster University, Hamilton, ON L8S 4M1, Canada
Received 2017 March 27; revised 2017 May 11; accepted 2017 May 12; published 2017 June 6

Abstract

Sub-subgiants (SSGs) are a new class of stars that are optically redder than normal main-sequence stars and fainter than normal subgiant stars. SSGs, as well as the possibly related red stragglers (which fall to the red of the giant branch), occupy a region of the color–magnitude diagram that is predicted to be devoid of stars by standard stellar evolution theory. In previous papers we presented the observed demographics of these sources and defined possible theoretical formation channels through isolated binary evolution, the rapid stripping of a subgiant's envelope, and stellar collisions. SSGs offer key tests for single- and binary-star evolution and stellar collision models. In this paper, we synthesize these findings to discuss the formation frequencies through each of these channels. The empirical data, our analytic formation rate calculations, and analyses of SSGs in a large grid of Monte Carlo globular cluster models suggest that the binary evolution channels may be the most prevalent, though all channels appear to be viable routes to SSG creation (especially in higher-mass globular clusters). Multiple formation channels may operate simultaneously to produce the observed SSG population. Finally, many of these formation pathways can produce stars in both the SSG and red straggler (and blue straggler) regions of the color–magnitude diagram, in some cases as different stages along the same evolutionary sequence.

Key words: binaries (including multiple): close – blue stragglers – globular clusters: general – open clusters and associations: general – stars: evolution – stars: variables: general

1. Introduction

This is the third paper in a series investigating the origins of a relatively new class of stars known as sub-subgiants (SSGs). In Geller et al. (2017, hereafter Paper I), we gather the available observations for these sources and find that SSGs share the following important empirical characteristics.

1. SSGs occupy a unique location on a color–magnitude diagram (CMD), redward of the normal main-sequence (MS) stars but fainter than the subgiant branch, where normal single-star evolution does not predict stars (see Figure 1).
2. More than half of the SSGs are observed to be X-ray sources, with typical luminosities of order $10^{30–31}$ erg s^{-1}, consistent with active binaries.
3. At least one-third of the SSGs exhibit Hα emission (an indicator of chromospheric activity).
4. At least two-thirds of the SSGs are photometric and/or radial-velocity variables, with typical periods of $\lesssim$15 days.
5. At least three-quarters of the variable SSGs are radial velocity binaries.
6. The specific frequency of SSGs increases toward lower-mass star clusters.

The fractions of sources given in items 2–5 above are all lower limits because not all sources have the necessary observations to investigate each characteristic.

In Leiner et al. (2017, hereafter Paper II), we study three specific formation channels in detail that can produce stars in the SSG region of the CMD, namely, (1) ongoing mass transfer from a subgiant donor, "SG MT"; (2) a reduced convective efficiency, likely related to increased magnetic activity, "SG Mag"; and (3) rapid and partial stripping of a subgiant's envelope, "SG Strip." Paper II also briefly considers a fourth channel, (4) a main-sequence–main-sequence (MS–MS) stellar collision, where the collision product is observed while settling back down onto the normal main sequence, "MS Coll." We provide details and models for these mechanisms in Paper II (and references therein) and describe them qualitatively in Section 2. For reference, in Figure 1 we show example evolutionary tracks for each of these mechanisms, plotted over an isochrone at the age of M67. Within this same figure we also define the SSG region on a CMD, with the dark-gray shading (see also Figure 1 in Paper I).

The "red straggler" (RS) stars, which are possibly related to the SSGs, are found in the region with the light-gray shading in Figure 1. We note here (and in Papers I and II) that there has been some confusion in the literature with the naming convention of these two types of stars. We urge readers to adopt the convention that we set forth in this series of papers to identify SSG and RS stars. There are far fewer RS stars than SSGs, but, despite their different location on the CMD, their empirical characteristics appear to be very similar to the SSG stars. Some of the SSG formation channels discussed in Paper II predict an evolutionary relationship between stars in the SSG and RS regions (where one is the precursor to the other), and furthermore at least two of the formation channels ("SG MT" and "MS Coll") can lead to the formation of a blue straggler star (BSS).

In this paper, we investigate the formation rates of SSGs through these four mechanisms using analytic calculations. Our goal is to identify if indeed all of these mechanisms are viable, or if one or more clearly dominate the production of SSGs. After

[6] NSF Astronomy and Astrophysics Postdoctoral Fellow.

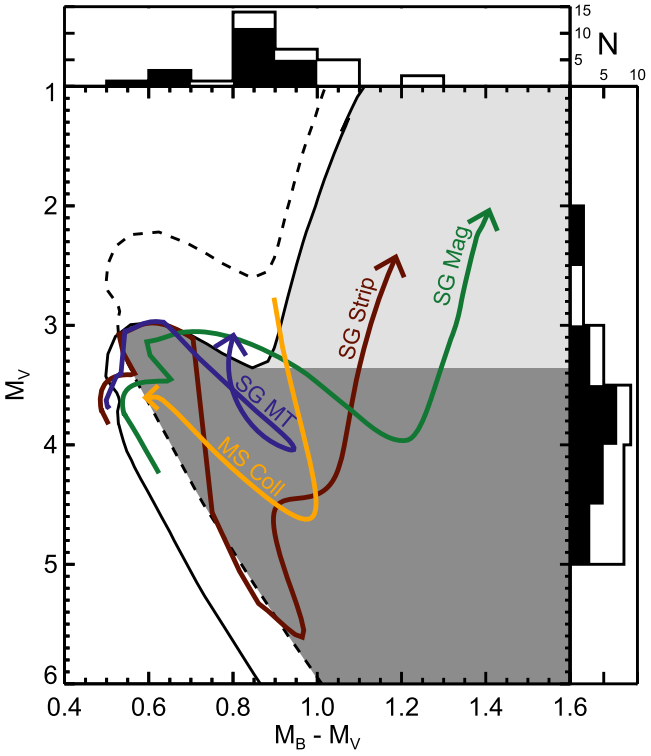

Figure 1. CMD showing the theoretical SSG formation channels (colored lines) and our definition of the SSG region (dark-gray shaded area) and RS region (light-gray shaded area), with respect to a PARSEC isochrone (Bressan et al. 2012) for M67 (solid line). In the main panel, the dashed line shows the equal-mass binary sequence for M67. We show evolutionary tracks from MESA (Paxton et al. 2015) for a subgiant undergoing stable mass transfer ("SG MT," purple line), a subgiant that has been stripped of much of its envelope (i.e., after ejecting a common envelope or after a grazing collision; "SG Strip," dark-red line), and a star that has a reduced convective mixing length coefficient (and increased magnetic activity; "SG Mag," green line). We also show the result of a collision between two 0.7 $M_\odot$ MS stars (from Sills et al. 2002; "MS Coll," yellow line). For all colored lines, the arrows indicate the direction of time along the evolutionary sequence. In the two subpanels, we show histograms of the observed distribution of SSG and RS stars from the open and globular clusters studied in Paper I, in M_V (right) and $M_B - M_V$ (top). The black filled histograms show the contribution from the globular cluster sources alone, with the additional white filled region (up to the solid lines) coming from the open cluster sources. We refer the reader to Figure 1 in Paper I for CMDs of these stars in the individual clusters.

providing a qualitative description of the four formation mechanisms in Section 2, we then discuss the probabilities of observing SSGs from each of these theoretical formation channels in Sections 3 and 4. We investigate SSGs created in *N*-body and Monte Carlo star cluster models in Section 5. Finally, in Section 6 we provide a brief discussion and conclusions.

2. Summary of Theoretical Formation Channels

In Paper II we study SSG formation channels in detail, primarily through in-depth analyses of MESA models (Paxton et al. 2015). In this section, we provide a brief summary of these formation channels, specifically for SSGs formed through ongoing binary mass transfer (Section 2.1), increased magnetic activity leading to inhibited convection (Section 2.2), rapid loss of an envelope (Section 2.3), and MS–MS collisions (Section 2.4). We refer the reader to Paper II for further details about the physics behind the first three mechanisms (and a wider exploration of parameter space). MS stellar collisions have been modeled previously in detail (e.g., Sills et al. 1997, 2001, 2002, 2005), in the context of BSS formation.

2.1. Ongoing Binary Mass Transfer Involving a Subgiant Star ("SG MT")

If a binary containing an MS star has a short enough orbital period (∼1.5 days for a circular binary with a primary star at the turnoff in M67), this MS star can overfill its Roche lobe shortly after evolving off of the MS. As mass transfer begins, the now subgiant star loses mass, becomes fainter, and moves into the SSG region.

The MESA model in Figure 1 shows a 1.0-day binary with a 1.3 $M_\odot$ primary and a 0.7 $M_\odot$ secondary. Mass transfer begins when the primary overflows its Roche lobe on the subgiant branch. Stable mass transfer proceeds with an efficiency of 50%. In this model, the binary remains in the SSG region for ∼400 Myr, which is comparable to the duration of the subgiant phase of a normal ∼1.3 $M_\odot$ star (of 600 Myr in MESA).

In this scenario, the subgiant must be the brighter star in the binary in the optical for it to appear in the SSG region. The accretor could be an MS star or a compact object. However, if an MS accretor is massive enough initially, it may gain enough mass to become a BSS, and dominate the combined light, before the subgiant becomes subluminous enough to enter the SSG region (unless the mass transfer is extremely nonconservative).

Here, one would expect to observe a short-period binary, likely with a rapidly rotating primary (subgiant) star. Photometric variability could potentially arise from ellipsoidal variations on the subgiant, spot activity, or eclipses. X-rays (and Hα emission) could be produced by chromospheric activity on the rapidly rotating subgiant and/or hot spots in the accretion stream onto a compact object (likely requiring a neutron star or black hole accretor to reach X-ray temperatures).

In many cases where the accretor is an MS star, the evolution will lead to the coalescence of the two stars, and interestingly, in this scenario, the merger product may be observed eventually as a BSS. The mass transfer model shown in Figure 1 eventually creates a BSS with a WD companion. Indeed, binary mass transfer is one of the primary BSS formation mechanisms (McCrea 1964; Tian et al. 2006; Chen & Han 2008; Geller & Mathieu 2011), especially in low-density ($\rho_c \lesssim 10^3 M_\odot\, pc^{-3}$) environments (Chatterjee et al. 2013a). We will come back to this potential connection between SSGs and BSSs in Section 6.

2.2. Increased Magnetic Activity in a Subgiant Star ("SG Mag")

While the effects of magnetic fields on stellar evolution are in general not well known, there is evidence that magnetic fields may alter the temperature and radii of stars by lowering the efficiency of convection. For example, low-mass eclipsing binaries are found to be larger and cooler than model predictions, which has been attributed to magnetic activity (e.g., Chabrier et al. 2007; Clausen et al. 2009). A similar mechanism may be at work in SSGs (Paper II). Chabrier et al. (2007) lower the mixing length coefficient in their models to mimic lowered convective efficiency. Our preliminary MESA models, where we reduce the convective mixing length coefficient to $\alpha = 1.2$ (see green line in Figure 1, and note that MESA's standard mixing length coefficient is $\alpha = 2.0$), suggest that this mechanism may produce SSGs primarily after the downturn on the subgiant branch and on

the lower red giant branch (RGB). Here, a close binary companion may tidally spin-up the subgiant star, causing the increased magnetic activity. The predicted tight binary and magnetic and chromospheric activity are consistent with the empirical SSG properties.

2.3. Rapid Loss of a Subgiant Star's Envelope ("SG Strip")

If the envelope of a subgiant star is rapidly stripped away, it will become fainter, while losing mass.[7] Once mass loss stops, the star will begin to evolve toward the subgiant and giant branches as before, but now along a path appropriate for its new lower mass. If enough mass is lost, the star will be fainter than the cluster's subgiant branch and eventually redder than the giant branch, moving through the observed SSG region.

For the "SG Strip" track shown in Figure 1, we use MESA to evolve a 1.3 $M_{\odot}$ star, and we remove 0.45 $M_{\odot}$ from the envelope soon after the star begins to evolve off of the MS and at a rate of 10^{-5} $M_{\odot}$ yr^{-1}. At this rate the star is driven out of thermal equilibrium initially, but it quickly returns to an equilibrium position once the removal of mass is complete. (This is the largest mass transfer rate we are able to reliably model in MESA for this stellar mass and evolutionary state; at larger rates hydrodynamical effects become important.)

One possible method to induce this rapid mass loss is a grazing collision between a subgiant and some more compact star (perhaps a compact object or MS star), with an impact parameter small enough to strip the subgiant's envelope, but large enough that the two stars do not directly merge. We will refer to this pathway as "SG Coll." A second potential method is through the ejection of a common envelope; we will refer to this pathway as "SG CE." For our purposes here, we do not consider what happens to the mass lost from the subgiant (whether it can be accreted by the other star or lost from the system entirely). Both of these mechanisms require further detailed modeling; here we will simply assume that they are both possible and will focus on the possibility of observing the product of such an event.

After both processes, a tight binary companion could remain (for the "SG Coll" scenario, this could be akin to a tidal capture; see, e.g., Fabian et al. 1975; Press & Teukolsky 1977). The subgiant may be spun up in this process. If the stripped subgiant is rotating rapidly, then one may expect to observe photometric variability and X-ray emission due to chromospheric activity and spots.

2.4. Collision of Two MS Stars ("MS Coll")

In Figure 1 we show a collision product from Sills et al. (1997) resulting from two 0.7 $M_{\odot}$ stars. Immediately after a collision between two MS stars, the collision product will become brighter (due primarily to the kinetic energy input from the motion of the stars leading up to collision) by a factor of about 10–50 (in luminosity) for the mass range of interest here. Afterward the star will settle back into thermal equilibrium by contracting and releasing gravitational potential energy, along analogous tracks to pre-MS stars. Through this contraction phase, the star becomes fainter and eventually settles back near the normal MS stars, but before reaching the MS the collision product may reside in the SSG region. The contraction phase occurs over roughly a thermal timescale, which is between about 1 and 15 Myr for the masses of interest here.

If the collision is off-axis, the product will likely be very rapidly rotating (Sills et al. 2005), which could lead to similar photometric variability and X-ray emission (particularly if a magnetic field can be maintained) to that observed for some SSGs. Scattering experiments and *N*-body star cluster simulations suggest that it would be difficult for the collision product to retain a binary companion at the short periods that are observed for many SSGs (i.e., of order 10 days) directly after a collision (e.g., Fregeau et al. 2004; Leigh & Sills 2011; Geller et al. 2013). Subsequent exchanges or tidal capture encounters could become more likely with the increased mass (and temporary increase in radius) of the collision product. Further scattering experiments and *N*-body models are necessary to better understand the likelihood for creating a short-period binary containing a collision product within such a short timescale after the collision (as would be required to produce SSGs in binaries with periods of order 10 days).

Though we show one specific collision model, a wide range of component masses can produce collision products in the SSG region. Furthermore, for certain combinations of MS stars, the collision product may be "born" in the RS region and contract through the SSG region as it settles back into thermal equilibrium. This mechanism has also been invoked to explain BSSs (e.g., Hills & Day 1976; Leonard 1989; Sills et al. 2009). A collision product that could be observed as an SSG may later be observed as a BSS, after the normal stars of similar mass evolve toward the subgiant and giant branches.

3. Probabilities of Observing the Products of Each Formation Channel

Each of these theoretical formation channels can produce products that have characteristics consistent with at least a subset of the observed SSGs. Many of these products are predicted to be relatively short-lived in relation to the age of the clusters that have SSGs. We investigate here the probability of observing at least one SSG from each mechanism, respectively, in different star clusters, both over a range in cluster masses (e.g., Figure 2) and for the observed parameters of the specific clusters that have SSGs (e.g., Table 1 and Figure 3).

We follow the same framework in our calculations for each mechanism, based on the cumulative Poisson probability:

$$\Psi(t, \tau) = 1 - e^{-(t/\tau)} \sum_{x=0}^{n-1} \frac{(t/\tau)^x}{x!}, \quad (1)$$

where t is the time interval of interest (here, the duration that the star remains in the SSG region), τ is the mean time in between events, and n is the number of events. Equation (1) gives the probability of observing n or more events over the time interval t, when the mean number of events is expected to be t/τ. We discuss our estimates for t and τ for each respective formation channel below, and in all cases we attempt to take the most optimistic assumptions.

First, our timescale calculations depend on the cluster age, mass (M_{cl}), metallicity ([Fe/H]), binary fraction (f_{b}), central velocity dispersion (σ_0), central density (ρ_0), core radius (r_{c}), and/or half-mass–radius (r_{hm}). We describe how we obtain these values in Section 4. In general, for our study of the specific

[7] Stripping the envelope of a red giant star has only a very minor affect on its luminosity (Leigh et al. 2016a), because the luminosity of a red giant is controlled almost entirely by the He core. Thus, despite the larger physical size of a red giant, and therefore the larger collision rate, this stripping mechanism may be most easily observed for subgiants.

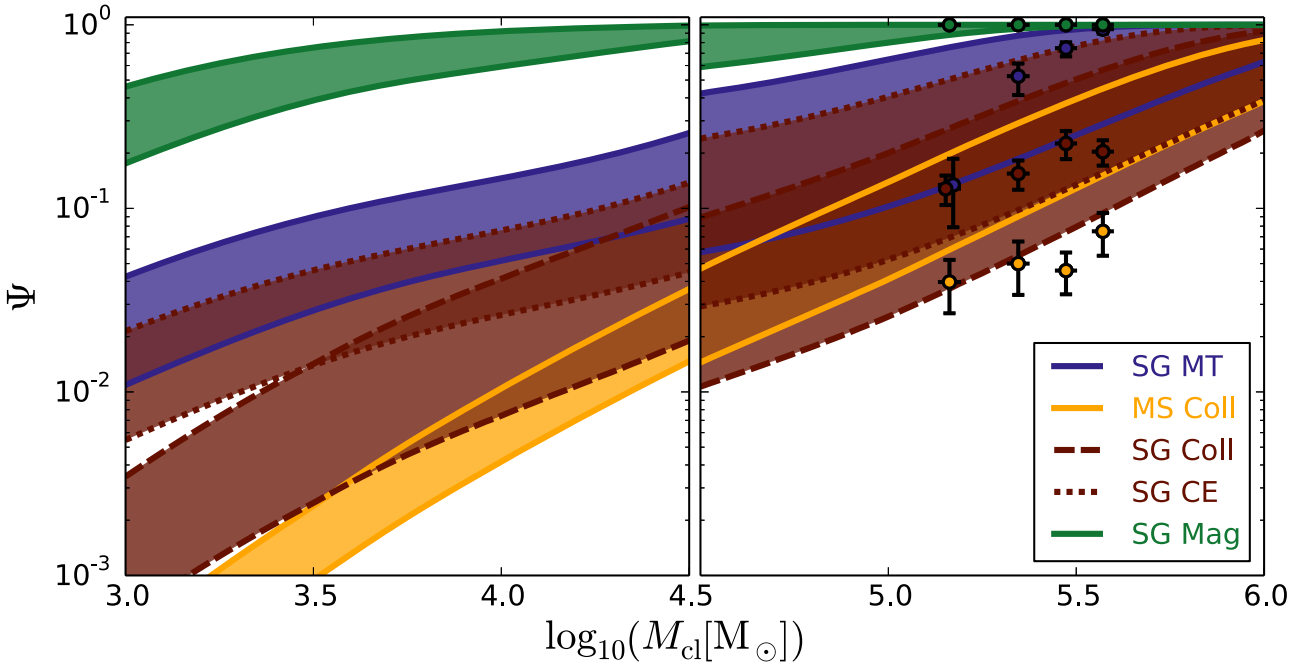

Figure 2. Poisson probabilities of observing SSGs resulting from the formation channels discussed in Section 2. "SG MT" (blue) is the probability of observing a binary in the process of mass transfer from a subgiant donor (Sections 2.1 and 3.1). "MS Coll" (yellow) is the probability of observing an MS–MS collision product before it settles back to the ZAMS (Sections 2.4 and 3.4). "SG Coll" and "SG CE" (red) are the probabilities of observing a subgiant after having its envelope rapidly stripped (Sections 2.3 and 3.3), either through a grazing collision (dashed) or through a common-envelope ejection (dotted). "SG Mag" (green) is the probability of observing a subgiant with a reduced convective mixing length from enhanced magnetic activity (Sections 2.2 and 3.2). Each region shows the Poisson probabilities derived from the weighted average timescales (t and τ from Equation (1)) over our grid of models, weighted by the observed distributions of ages, half-mass radii, and metallicities for open clusters (left) and globular clusters (right), as described in Sections 3 and 4.1. The widths show one (weighted) standard deviation above and below the weighted mean. Additionally, we plot predictions from globular cluster Monte Carlo models for the probability of observing SSGs created through each channel (see Section 5): points show the weighted means, vertical error bars show the standard errors of the mean, and horizontal bars show the widths of each mass bin. (Mass bins are the same for each channel; for the lowest-mass bin of the "SG MT" and "SG Coll" channels, we shift the points slightly for readability.)

clusters (Section 4.2), we obtain values from the literature (Table 1). For our general calculations (Section 4.1, and also as estimates for cluster-specific values that are unavailable in the literature), we assume a Plummer (1911) model and also use the semianalytic cluster evolution code EMACSS (Alexander & Gieles 2012; Alexander et al. 2014; Gieles et al. 2014).

To start, we use the rapid Single Star Evolution code SSE (Hurley et al. 2000) to determine the mass of a star that would reside at the base of the giant branch for a given cluster age and metallicity. We take the evolutionary states for stars in these calculations directly from SSE. We will refer to this star as S_1 below. We then use SSE to determine the mass, radius, and luminosity of this star when it was on the zero-age main sequence (ZAMS), the terminal-age MS, and at the base of the RGB, for a given metallicity.

For many of the scenarios, we also require the number of subgiants (or the fraction of stars that are subgiants, $f_{\rm SG}$) expected to be in a given cluster. To estimate this value, we first determine an appropriate mass function of a cluster of a given age and mass using the method of Webb & Leigh (2015), which accounts for the change to a Kroupa (2001) initial mass function (IMF) due to dynamical evolution and mass loss from the cluster.[8] This method requires an estimate of the initial cluster mass, which we derive by iteratively modeling clusters of different initial masses using EMACSS until reproducing the observed present-day cluster mass (at either the solar galactocentric distance, for Section 4.1, or the true galactocentric distance of the given cluster, for Section 4.2). We then use SSE to estimate the masses of stars that would evolve off the MS at ± 1 Gyr from the cluster age. These masses, combined with the mass function, provide a rate at which stars evolve off the MS at the given cluster age and metallicity, $\Gamma_{\rm ev}$. This rate multiplied by the lifetime of S_1 on the subgiant branch yields an estimate of the number of subgiant stars in a given cluster (and a similar method can provide the number of MS stars in the cluster).

This theoretical estimate for the number of subgiants is consistent with observed values. For instance, in the open clusters studied in Paper II, we count 20–30 subgiant stars in M67 and about 100 subgiant stars in NGC 6791. (These numbers, of course, depend on where one defines the end of the MS and the base of the RGB, which can be somewhat subjective on a CMD.) Following the theoretical procedure above, we predict 32 subgiants in M67 and 120 in NGC 6791, both consistent with the observed values.

Given the mass function, we can also estimate the mean single-star mass in the cluster, $\langle m_{\rm s}\rangle$. For some calculations, we also desire the mean mass of an object (single or binary). We estimate this value as $\langle m\rangle = (1-f_{\rm b})\langle m_{\rm s}\rangle + f_{\rm b}\langle m_{\rm b}\rangle$, where $f_{\rm b}$ is the cluster binary fraction, $\langle m_{\rm b}\rangle$ is the mean binary mass, and we assume a mean binary mass ratio of 0.5 (a reasonable guess for an approximately uniform mass ratio distribution, as is observed for solar-type binaries in the Galactic field and globular clusters; see, e.g., Raghavan et al. 2010 and Milone et al. 2012) such that $\langle m_{\rm b}\rangle = 1.5\langle m_{\rm s}\rangle$.

[8] The true cluster mass function depends on many uncertain factors (e.g., the IMF, initial Jacobi filling factor, remnant retention fractions) that are neglected in the simplified Webb & Leigh (2015) relation. However, this simplified relation is sufficient for the approximate calculations performed here.

Table 1
Sub-subgiant Formation Probabilities

Cluster	Age (Gyr)	[Fe/H]	M_{cl} ($M_\odot$)	f_b	σ_0 (km s^{-1})	$\log(\rho_0)$ ($M_\odot$ pc^{-3})	r_c (pc)	r_{hm} (pc)	P_{circ} (day)	n_{SSG}	$\Psi_{SG\ MT}$	$\Psi_{MS\ Coll}$	$\Psi_{SG\ Coll}$	$\Psi_{SG\ CE}$	$\Psi_{SG\ Mag}$	$\Psi(n_{SSG})$
Open Clusters																
NGC 188	6.2	0.0	1500 ± 400	0.5 ± 0.05	0.41 ± 0.04	⋯	2.1	4.0	14.5 ± 1.8	3	0.042	0.003	0.02	0.02	0.5	0.04
NGC 2158	2	−0.6	15000	⋯	⋯	⋯	3.23	⋯	⋯	1	0.05	0.006	0.001	0.026	0.27	0.33
NGC 2682	4	0.0	2100 ± 600	0.57 ± 0.04	0.59 ± 0.07	⋯	1	⋯	12.1 ± 1.3	2	0.05	0.05	0.1	0.0	0.47	0.2
NGC 6791	8	0.4	4600 ± 1500	⋯	0.62 ± 0.1	⋯	3.4	⋯	⋯	5	0.086	0.004	0.03	0.04	0.82	0.04
NGC 6819	2.4	0.0	2600	0.4 ± 0.02	⋯	⋯	1.75	⋯	6.2 ± 1.1	1	0.016	0.005	0.001	0.008	0.12	0.15
NGC 7142	3.6	0.1	500	⋯	⋯	⋯	3.1	⋯	⋯	0	0.009	0.00013	0.0003	0.0045	0.1	⋯
Globular Clusters																
NGC 104	13.1	−0.72	1.0×10^6	0.02 ± 0.01	11 ± 0.3	5.18	0.47	4.15	⋯	8	0.71	1	1	0.46	1	1
NGC 5139	11.5	−1.53	2.2×10^6	⋯	16.8 ± 0.3	3.45	3.59	7.56	⋯	15	0.99	0.4	0.4	0.9	1	1
NGC 6121	12.5	−1.16	1.3×10^5	0.1 ± 0.01	4 ± 0.2	3.94	0.74	2.77	⋯	2	0.4	0.73	0.85	0.25	1	1
NGC 6218	12.7	−1.37	1.4×10^5	0.06 ± 0.01	4.5 ± 0.4	3.53	1.10	2.47	⋯	1	0.38	0.3	0.4	0.2	1	1
NGC 6366	13.3	−0.59	4.8×10^5	0.11 ± 0.03	1.3 ± 0.5	2.70	2.21	2.98	⋯	1	0.6	0.2	0.4	0.4	1	1
NGC 6397	12.7	−2.02	7.7×10^4	0.02 ± 0.01	4.5 ± 0.2	6.06	0.03	1.94	⋯	3	0.07	0.5	0.3	0.0	0.5	0.3
NGC 6652	12.9	−0.81	7.9×10^4	0.1 ± 0.01	⋯	4.78	0.29	1.40	⋯	0	0.89	0.89	1	0.68	1	⋯
NGC 6752	11.8	−1.54	2.1×10^5	0.01 ± 0.01	4.9 ± 0.4	5.34	0.20	2.22	⋯	0	0.1	0.97	0.97	0.05	0.6	⋯
NGC 6809	12.3	−1.94	1.8×10^5	⋯	4 ± 0.3	2.52	2.83	4.45	⋯	2	0.43	0.07	0.04	0.25	0.99	0.98
NGC 6838	12.0	−0.78	3.0×10^4	0.22 ± 0.02	2.3 ± 0.2	3.13	0.73	1.94	⋯	2	0.33	0.13	0.4	0.2	1	1

Note. References for the values in this table, other than the probabilities, are as follows. For the open clusters: NGC 188—we take the age from Meibom et al. (2009) and the adopted [Fe/H] from Sarajedini et al. (1999), M_{cl}, r_c, r_{hm} from Chumak et al. (2010), f_b from Geller et al. (2013), σ_0 from Geller et al. (2008), and P_{circ} from Meibom & Mathieu (2005). NGC 2158—we take the age, [Fe/H], M_{cl} from Carraro et al. (2002), and r_c from Kharchenko et al. (2013). NGC 2682—we take the age, [Fe/H], M_{cl}, f_b, σ_0, r_c from Geller et al. (2015, and references therein), and P_{circ} from Meibom & Mathieu (2005). NGC 6791—we take the age, [Fe/H] from Carney et al. (2005), M_{cl}, σ_0 from Tofflemire et al. (2014), and r_c from Platais et al. (2011). NGC 6819:—we adopt the age, [Fe/H] from Hole et al. (2009, and references therein), take M_{cl}, r_c from Kalirai et al. (2001), and f_b (scaled here to include the full period distribution using the method from Geller et al. 2015), P_{circ} from Milliman et al. (2014). NGC 7142—we take the age, [Fe/H] from Sandquist et al. (2013, and references therein), estimate M_{cl} from Straižys et al. (2014), and take r_c from Kharchenko et al. (2013). For the globular clusters: we take the age from Marín-Franch et al. (2009, using the "$G00_{CG}$" values and normalized using the age of 47 Tuc from Thompson et al. 2010), [Fe/H], σ_0 (where available), M_{cl} and $\log\rho_0$ (both calculated assuming a mass-to-light ratio of 2), r_c, r_{hm} from Harris (1996, 2010), and f_b (where available) from Milone et al. (2012). For NGC 6366 we calculate the mass from σ_0 assuming a Plummer model. Finally, for NGC 6838 we take the age from Di Cecco et al. (2015).

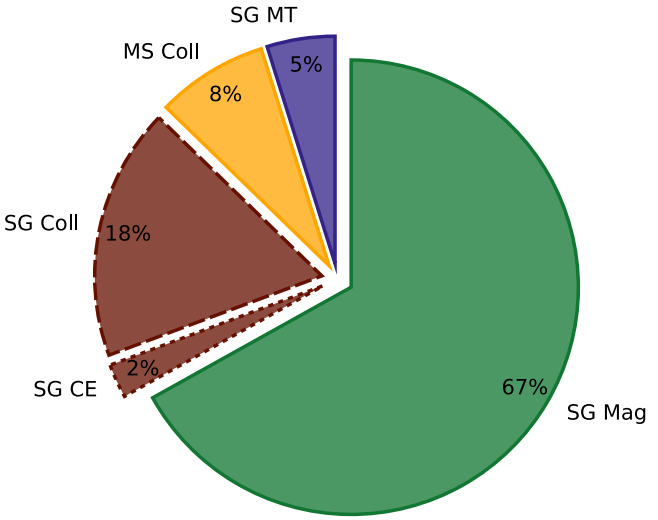

Figure 3. Percent of total SSGs predicted from each formation mechanism (see Sections 2 and 3) in all the observed clusters in Table 1.

For our general calculations, discussed in Section 4.1, we obtain the binary frequency, f_b, for globular clusters from the empirical study of Leigh et al. (2013). For open clusters, we estimate f_b by first assuming that prior to dynamical disruptions the binaries would follow the field solar-type stars, with a 50% binary frequency and a log normal binary period distribution (Raghavan et al. 2010, with a mean of $\log(P\,[\mathrm{days}]) = 5.03$ and $\sigma = 2.28$). Then we truncated the period distribution at the hard–soft boundary,

$$P_{\mathrm{hs}} = \frac{\pi G}{\sqrt{2}}\left(\frac{m_1\langle m_s\rangle}{\langle m\rangle}\right)^{3/2}(m_1 + \langle m_s\rangle)^{-1/2}\sigma_0^{-3}, \quad (2)$$

derived using the virial theorem to relate the mean binary binding energy to the local mean kinetic energy of an incoming star, where m_1 is the initial mass of S_1 and σ_0 is the three-dimensional velocity dispersion in the core (and we assume a Plummer [1911] model and that $\sigma_0 = \sqrt{3}\,\sigma_{0,1D}$). We calculate the cluster binary frequency as the ratio of the area under the truncated period distribution to that of the full distribution times the 50% solar-type field binary frequency. This assumes that the cluster has lived through sufficient relaxation times that all binaries have cycled through the core, which is reasonable for the open clusters known to contain SSGs. (A more detailed calculation might account for the time and radial dependence of the hard–soft boundary, but that is beyond the scope of this paper.) This produces binary fractions consistent with open cluster observations (e.g., Geller & Mathieu 2012; Geller et al. 2015). In practice, this method for open clusters requires an iterative derivation of f_b, $\langle m\rangle$, and P_{hs}. For our cluster-specific calculations, discussed in Section 4.2, we take the observed binary fractions (where available).

In the following, we describe our derivation of the timescale τ from Equation (1) for each specific formation mechanism. For the MS–MS collision channel, we also derive t, while for all others we simply take t equal to the lifetime of S_1 on the subgiant branch. Again, our assumption for t represents the most optimistic scenario for the duration of each mechanism.

3.1. Ongoing Binary Mass Transfer Involving a Subgiant Star

We calculate τ here as the mean time between stars in appropriate binaries evolving off of the MS. Only binaries with orbital periods large enough to avoid Roche lobe overflow (RLOF) on the MS and small enough to undergo RLOF on the subgiant branch are of interest, which defines a fraction of the binary population by period f_P. Here, we use the Roche radius equation from Eggleton (1983):

$$\frac{r_L}{a} = \frac{0.49q^{-2/3}}{0.6q^{-2/3} + \ln(1 + q^{-1/3})}, \quad (3)$$

where we set $q = \langle m_s\rangle/m_1$, a is the binary's semimajor axis, and we assume circular orbits (a standard assumption, given the expectation of tidal circularization, and sufficient for these approximate calculations). Likewise only binaries expected to undergo stable mass transfer are of interest. We impose a critical mass ratio of $q_{\mathrm{crit}} = m_{\mathrm{accretor}}/m_{\mathrm{donor}} = 1/3$, below which we assume that the system undergoes a common envelope and is not included in this particular mechanism. The value of $1/3$ is similar to values used in binary population synthesis codes for such stars (e.g., Hurley et al. 2002; Belczynski et al. 2008; see also Geller et al. 2013; Eggleton 2006). Assuming a uniform mass ratio distribution, this critical mass ratio allows only $2/3$ of the binaries to potentially undergo stable mass transfer and thereby provides a factor of $f_q = 2/3$ below. These factors, multiplied by the rate at which stars evolve off the MS at the given cluster age and metallicity (Γ_{ev}, see Section 3), yield

$$\tau_{\mathrm{SG\ MT}} = (\Gamma_{\mathrm{ev}} f_b f_P f_q)^{-1}. \quad (4)$$

3.2. Increased Magnetic Activity in a Subgiant Star

To calculate τ, we follow a similar method as in Section 3.1 to estimate the mean time between stars in appropriate binaries evolving off of the MS. Here, for f_P, we set the short-period limit to be that at the Roche radius (see Equation (3), thereby excluding any binaries included in Section 3.1) and the long-period limit to the binary circularization period of the cluster. We estimate the circularization period of a cluster of a given age from the results of Geller et al. (2013, dotted line in their Figure 2, which matches the observed binary circularization periods from Meibom & Mathieu 2005). The fraction of binaries with these short periods defines f_P. We allow all mass ratios here.

However, not all short-period binaries containing a subgiant star must become SSGs. A sample of the open clusters (NGC 188, NGC 2682, NGC 6819, and NGC 6791) have sufficient time-series radial velocity and/or photometric observations to count the known binaries with orbital periods less than 15 days among the SSGs and subgiants, as a rough estimate of the efficiency of SSG formation through this mechanism. Within these clusters, we find four normal subgiants and nine SSGs, respectively, in binaries with periods <15 days. We apply this fraction of $\alpha = 9/13$ to our calculation:

$$\tau_{\mathrm{SG\ Mag}} = (\alpha\Gamma_{\mathrm{ev}} f_b f_P)^{-1}. \quad (5)$$

Finally, as noted above, here we again simply take t as the lifetime of S_1 on the subgiant branch. It is possible that such stars can remain in the SSG region also during the early evolution of the red giant phase. Adding this to t would increase our probabilities of observing an SSG from "SG Mag."

3.3. Rapid Mass Loss from a Subgiant Star

Here we investigate two stripping mechanisms: through (i) common envelope or (ii) a grazing collision. For the common-envelope case, "SG CE," we use nearly the same calculations as for the "SG MT" channel (Section 3.1), but here we set $f_q = 1/3$ in Equation (4). This optimistic scenario assumes that every subgiant that undergoes a common envelope will have its envelope stripped in such a way as to produce an SSG.

For the grazing collision case, "SG Coll," τ is the mean time between collisions involving the stars of interest:

$$\tau_{\rm SG\ Coll}(a) = [f_{\rm SG}(2\Gamma_{11} + 3f_{c12}\Gamma_{12}(a) + 4f_{c22}\Gamma_{22}(a))]^{-1}, \quad (6)$$

where Γ_{11}, Γ_{12}, and Γ_{22} are the single–single, single–binary, and binary–binary encounter rates from Leigh & Sills (2011),[9] and $\tau = 1/\Gamma$, except here we multiply each rate by a factor, $(Nf_{\rm SG})$, to account for the requirement that at least one of the stars involved must be a subgiant, where $N = 2, 3, 4$ is the number of stars in the encounter and $f_{\rm SG}$ is the fraction of stars in the cluster that are expected to be subgiants (as explained above). f_{c12} and f_{c22} are the fractions of $1 + 2$ and $2 + 2$ encounters, respectively, that result in direct collisions, taken from the grid of scattering experiments of Geller & Leigh (2015) for a given cluster mass and half-mass radius. As these scattering experiments only include MS stars, we multiply these factors by the ratio of the gravitionally focused cross section for S_1 to that of an MS star at the turnoff (i.e., $(M_{S_1}R_{S_1})/(M_{\rm MSTO}R_{\rm MSTO})$; Leonard 1989).

Γ_{12} and Γ_{22} both depend on the binary semimajor axis, a (or orbital period), and we allow binaries from the Roche limit of S_1 on the ZAMS up to the hard–soft boundary (thereby excluding encounters with soft binaries). To calculate $\tau_{\rm SG}$ for Equation (1), we take the average of $\tau_{\rm SG\ Coll}(a)$, weighted by the log normal period distribution (within the appropriate Roche limit and hard–soft boundary).

We assume here that each collision results in sufficient stripping to produce an SSG. This is likely an overestimate of the true SSG production rate through this mechanism. Again, we aim for the most optimistic assumptions in our calculations here.

Finally, as mentioned above, we set $t_{\rm SG\ Strip}$ equal to the lifetime of S_1 on the subgiant branch. In our exploratory MESA modeling in Paper II, we see that for different amounts of stripping, and for different assumptions about the time the stripping occurs, the product can have a lifetime in the SSG region that is somewhat greater than, or less than, the subgiant lifetime of S_1. Accounting for this level of detail is beyond the scope of this paper, but may warrant future investigation.

3.4. Collision of Two MS Stars

To estimate t here, we start with the mean time of all collision products in Sills et al. (1997) to evolve from immediately after the collision back to the ZAMS, $t_{c0} = 6.74$ Myr. The mean increase in luminosity for all collision products in Sills et al. (1997) from immediately after the collision until settling back to the MS is a factor of $10^{1.5}$, and we assume this increase for all collision products in our calculations. We then make the simplifying assumption that the product's luminosity decreases linearly in time. Finally, we step through bins in stellar mass and calculate a weighted average of the time that an MS–MS collision product is estimated to remain in the SSG region for a given cluster:

$$t_{\rm MS\ Coll} = \frac{\sum_{m=m_0}^{m_f}\left(\frac{6.74}{[\rm Myr]}\right)f(m)w(m)}{\sum_{m=m_0}^{m_f}w(m)}, \quad (7)$$

where $w(m)$ weights by the mass function at the mass m, m_f is the ZAMS mass of S_1, and m_0 is the mass of an MS star with a luminosity that is $10^{1.5}$ times smaller than m_f (from SSE). The factor $f(m)$ is an estimate of the fraction of the time from collision to ZAMS that the product is expected to remain in the SSG region; this factor follows from our assumption that the luminosity of the product immediately after the collision increases by a factor of $10^{1.5}$ and then decreases back to the ZAMS linearly with time, and it may pass through the SSG region that extends from the magnitude of the main-sequence turnoff down to 1.5 mag fainter (approximately covering the region of observed SSGs; see Figure 1). Certainly a more detailed treatment of this factor is desirable, but it is beyond the scope of this paper.

We follow the same approach to calculate $\tau_{\rm MS\ Coll}$ as in Section 2.3, but we take f_{c12} and f_{c22} directly from Geller & Leigh (2015) and use the fraction of MS stars with masses between m_0 and m_f, in place of the fraction of subgiant stars ($f_{\rm SG}$), in the cluster.

4. Comparison of the Probabilities of Observing Each Product

We use two methods to compare the probabilities of observing at least one product of each respective formation channel (given the two timescales for each channel discussed above): one general and averaged over all observed open and globular clusters as a function of cluster mass (Section 4.1 and Figure 2), and the other specific to each cluster with observed SSGs (Section 4.2, Table 1, and Figure 3).

4.1. General

We begin by producing a grid of timescales (t and τ from Equation (1)) for each mechanism covering the range of relevant cluster ages (from 2 to 13 Gyr, in steps of 1 Gyr), masses (from $\log(M_{\rm cl}\ [M_\odot]) = 3$ to 6, in steps of 0.01), half-mass radii (from $r_{\rm hm} = 1$ to 10 pc in steps of 1 pc), and metallicities (from [Fe/H] $= -2.3$ to 0.2, with steps of 0.5 for [Fe/H] between -2 and 0; the metallicity range possible in SSE is $Z = [0.0001, 0.03]$, which corresponds to [Fe/H] $\sim [-2.3, 0.2]$) for observed open and globular clusters. We use a Plummer model and EMACSS, where necessary, as well as the assumptions discussed in Section 2.

We then compile all available observed values of age, $r_{\rm hm}$, and [Fe/H] for open (Salaris et al. 2004; van den Bergh 2006)[10] and globular (Harris 1996, 2010; Marín-Franch et al. 2009) clusters. Then for each of these two samples, we take a

[9] The encounter rates depend on the binary fraction, core radius, stellar density, velocity dispersion, mean stellar mass, and physical size of the object (i.e., the stellar radius for a $1 + 1$ encounter and the semimajor axis for the $1 + 2$ or $2 + 2$ encounter). We describe how we estimate these values in Section 3.

[10] We note that a larger catalog for these parameters exists in Piskunov et al. (2008) and Kharchenko et al. (2013), but here we are more interested in the older open clusters, like those observed to have SSGs, which were more carefully analyzed and provided in the given references.

weighted average of our calculated grid of timescales for each respective mechanism, weighted by the fraction of open or globular clusters within each bin of age, $r_{\rm hm}$, and [Fe/H]. Finally, we use these weighted average timescales to calculate the Poisson probabilities of observing at least one SSG within a cluster of the given mass. We divide our results at a mass of 10^4 $M_\odot$, which separates our sample at roughly the transition mass between open and globular cluster mass.

The resulting probabilities for each SSG formation mechanism are shown in Figure 2, in the different colored regions with widths equal to one (weighted) standard deviation from the weighted mean value. In general, taking $1/\Psi$ gives the number of clusters that should be observed in order to expect to detect at least one SSG from the given mechanism. Our calculations predict that roughly one in every few open clusters and nearly every globular cluster should host at least one SSG. This is in reasonable agreement with the current state of observations (see Figure 4 and Section 4.2), though no systematic survey for SSGs exists (in open or globular clusters). As we have taken optimistic assumptions in our calculations, these probabilities may be interpreted as upper limits.

Our calculations predict that the probability of observing SSGs from all mechanisms will increase with increasing cluster mass. This is simply due to the larger number of stars. More importantly, for clusters of all masses, we predict that isolated binary evolution mechanisms are dominant. The other mechanisms follow at lower probabilities; however, toward the highest-mass globular clusters, it becomes equally likely to observe at least one SSG from all mechanisms.

Although we show in Figure 2 the probabilities of observing SSGs as a function of cluster mass, cluster density (and encounter rate) is also important. For a given cluster mass, the rate of SSG formation through the collision channels increases with increasing density, while the rate of SSG formation through the binary evolution mechanisms is nearly independent of density (within the range of parameters relevant to observed open and globular clusters). The only dynamical mechanism that can affect the binary evolution channels in these calculations is the truncation of the binary orbital period distribution at the hard–soft boundary, which, for clusters of interest, is at longer periods than the synchronization period (and the period at RLOF). Again, these are optimistic assumptions meant to provide an upper limit on SSG formation rates. As we discuss below, more subtle dynamical effects, like perturbations and exchanges, within hard binaries may decrease the true SSG production rate through the binary evolution channels for the most massive clusters.

4.2. Cluster Specific

In addition to the general calculation described above, we also perform specific calculations of the respective probabilities to observe at least one product of each of the formation channels for each cluster with an SSG candidate. Here we compile all available data for each cluster that would serve as an input into our probability calculations described in Section 3, and we provide these in Table 1. As described above, our calculations require the age, mass, metallicity, and either the core or half-mass radius. Where available, we provide the additional empirical input to our calculations of the observed binary frequency ($f_{\rm b}$), central density (ρ_0), core radius ($r_{\rm c}$), half-mass radius ($r_{\rm hm}$), and circularization period ($P_{\rm circ}$). All other

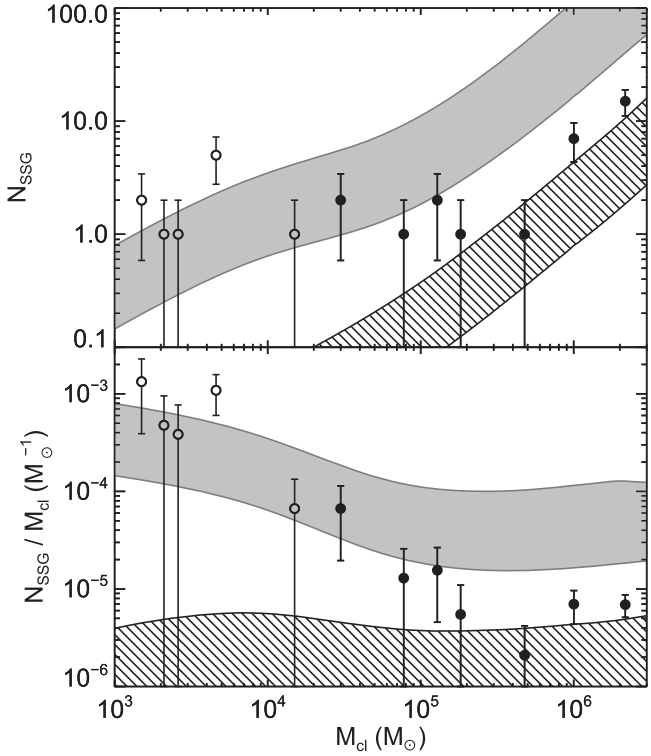

Figure 4. Number (top) and specific frequency (bottom; number of SSGs, $N_{\rm SSG}$, divided by the cluster mass, $M_{\rm cl}$) of SSGs as a function of the cluster mass. Observed open/globular clusters from Paper I are plotted in open/filled symbols. As in Paper I, we show only those observed SSGs with the highest likelihood of cluster membership and within the same radial completeness limit of <3.3 core radii (see Paper I for details). Error bars show the standard Poisson uncertainties on $N_{\rm SSG}$ (and we truncate the lower error bars for cases with $N_{\rm SSG} = 1$). The gray filled region shows the predicted number of SSGs from our calculations in Section 4.1 through all mechanisms combined, and the hatched region shows the predicted number of SSGs for the collision mechanisms alone (i.e., "SG Coll" and "MS Coll"). Note that our Poisson calculations are not limited in radius from the center of the cluster (as are the observations) and rely on optimistic assumptions; these calculations show upper limits.

necessary values that are unavailable in the literature are inferred using the same assumptions as above.

We use these empirical values to determine t and τ in Equation (1), as described in Section 3, and provide the probabilities of observing at least one SSG from the given mechanism in each cluster in Table 1. We also provide the combined Poisson probabilities of observing the observed number of SSGs ($n_{\rm SSG}$) in each cluster[11] from any formation channel (calculated by summing the t/τ values from each mechanism and using this in Equation (1), and only given for clusters with SSGs). For ease of reading, we do not include uncertainties on these probabilities in the table; however, we do follow the uncertainties on each input parameter through our calculations for each probability. If a parameter does not have uncertainties in the literature (and therefore no error is given in the table), we assume a 10% uncertainty for our calculations. The number of digits provided in the table shows the order of magnitude of the inferred range in probabilities resulting from

[11] The number of SSGs is taken from Paper I, where we select stars that reside in the SSG region of the CMD in at least one available color–magnitude combination and have a <10% probability of being a field star.

the uncertainties in input values. We round any probability >0.99 up to 1.

In Paper II, we investigate the SSGs in two of these clusters, NGC 6791 and M67, in depth and perform more careful calculations of their formation (involving more detailed empirical input and using a slightly different method). Our results here agree very well with those from Paper II, which provides further confidence in our calculations here. Specifically, in Paper II we find a probability of observing at least one SSG from the "SG MT" mechanism in M67 of 4% and in NGC 6791 of 14%, where here we find 5% and 9%, respectively. In Paper II, we find a probability of 42% and 94% of observing at least one SSG from the "SG Mag" in M67 and NGC 6791, respectively, as compared to 47% and 82% here. For the "SG Coll" scenario, in Paper II we find a probability of ∼3% that we would observe at least one in M67, compared to 20% here. Though this particular probability value appears higher here (due to our more optimistic assumptions), the uncertainty on this probability is of the same order as the value itself.

Additionally, we show the results graphically in Figure 3, where we plot the percentage of SSGs predicted, over all clusters in Table 1, to come from each mechanism. To construct this plot, we sum the number of predicted SSGs for a given mechanism over the observed clusters and divide by the total number of SSGs predicted for all clusters from all mechanisms. For instance, our calculations predict that 67% of SSGs in these observed clusters may come from the "SG Mag" mechanism.

Nonetheless, if we sum the probabilities for each mechanism given in Table 1, we expect to observe at least one SSG from each mechanism when considering all clusters. For nearly all of the globular clusters our calculations suggest that these formation channels are sufficient to explain all observed SSGs (i.e., $\Psi_{\rm nSSG} \sim 1$ for these clusters). In the open cluster regime, the number of SSGs predicted for clusters in this mass range is in rough agreement with the observations (Figure 4), though the specific $\Psi_{\rm nSSG}$ values for the observed open clusters are below 1 in Table 1. This may indicate that we have overlooked viable formation channels in the open cluster regime or that we have underestimated values in our calculations primarily for open clusters, and we return to this in Section 6.

In Figure 4 we show the number of SSGs predicted by our model as a function of cluster mass, compared to that of the observed clusters (see Paper I, Figure 7). The gray band combines all formation channels, while the hatched region shows only the collision channels. Our model agrees with the general trend in the observations, of decreasing specific frequency of SSGs toward increasing cluster mass. However, toward the high-mass end, our model begins to overpredict the number of SSGs. This may imply that there are more SSGs to be discovered in these clusters (which indeed is expected; see Paper I). This discrepancy may also be tied, at least in part, to our simplified treatment of how dynamics affects the binary evolution channels. Perhaps more subtle dynamical effects (such as perturbations or exchanges, not included in these calculations) inhibit the binary evolution channels significantly in clusters with high encounter rates (like the massive observed clusters in our sample). We investigate this further in the following section. Indeed, for the most massive clusters in our sample, our model predicts that the collision mechanisms alone can nearly produce the observed numbers of SSGs.

5. SSGs in Star Cluster *N*-body Models

Our Poisson probability calculations make simplifying assumptions about SSG formation and provide upper limits for SSG formation rates. *N*-body star cluster models can alleviate some of these simplifications and in particular can allow us to study the effects from more complex dynamical encounters and subtle perturbations, which we do not consider in our analytic calculations.

5.1. Direct N-body Models

To our knowledge, the Hurley et al. (2005) *N*-body model of M67 is the only star cluster model that specifically discusses the creation of an SSG star. They used the NBODY4 code (Aarseth 1999), which utilizes BSE (Hurley et al. 2002) for binary-star evolution. The only pathway available for SSG formation in these models is through binary evolution; the other mechanisms discussed here are not yet implemented in the *N*-body code for SSG formation (though some are implemented to produce BSSs).

This specific binary first went through a stage of conservative stable mass transfer, where the subgiant primary transferred mass onto its MS companion. This then led to a common-envelope merger event that created the SSG single star seen at the age of M67. (We refer the reader to Hurley et al. (2005) for a more detailed description of this star's history.) This mechanism is similar, in part, to our "SG MT" pathway (Section 2.1) and is formally included in the "SG MT" rate calculations described in Sections 3 and 4 (because the system starts with stable mass transfer). Unlike our mechanism, however, the Hurley et al. (2005) star is more massive than the normal giants in the cluster at the age of M67, but with a lower core mass than the normal giants. They attribute the lower luminosity of the object to this lower core mass. Through our extensive BSE modeling (see Paper II), we do not see common-envelope merger products as a dominant SSG formation channel within the mass transfer mechanism, though we have likely not covered the entire parameter space leading to SSG formation in BSE (and common-envelope evolution remains poorly understood and only approximated within BSE). Furthermore, as most of the observed SSGs in open clusters appear to be in short-period binaries, this specific pathway may not produce SSGs similar to the majority of those observed.

5.2. Monte Carlo Models

We also investigated a grid of Monte Carlo globular cluster models, from the Northwestern group (Joshi et al. 2000, 2001; Fregeau et al. 2003; Fregeau & Rasio 2007; Chatterjee et al. 2010; Umbreit et al. 2012). Specifically, we use a superset of the simulations presented in Chatterjee et al. (2010, 2013a, 2013b), which includes 327 models that cover the parameter space of the observed globular clusters in our Galaxy (though all at a metallicity of $Z = 0.001$). We examine snapshots from these models between 9 and 12 Gyr. We used two methods to identify SSGs in these models: (1) we selected SSGs based on the location in the H-R diagram (as in Figure 1), and (2) we identified other stars that may be observed as SSGs in a real cluster, but were not found in the SSG region of the simulated H-R diagram owing to limitations of BSE (which is used in both the NBODY4 and Monte Carlo models).

Method (1) discovers all SSGs produced through the "SG MT" channel; this is the only mechanism available for producing SSGs within BSE. We identified over 1100 "SG MT" SSGs in these models; 99% of these simulated SSGs are currently in binaries, and the remainder were previously in binaries. Further, 98% of the SSGs in binaries are currently undergoing RLOF. Of the few that are detached, ∼80% contain an evolved star that had previously lost $\geqslant 0.1 M_{\odot}$, presumably from a recently completed period of mass transfer (a subpopulation that we also briefly discuss in Paper II). Importantly, only ∼10% of these SSGs suffered strong encounters or direct collisions prior to becoming an SSG (though weak flybys are not tracked in these models, as this is part of the relaxation process). The vast majority of "SG MT" SSGs in these models avoided strong encounters for the entire lifetime of the globular cluster.

To investigate predictions for the other formation channels, we follow similar assumptions as in Section 3. More specifically, we identify "SG Mag" SSGs as binaries in the models with orbital periods $P < P_{\rm circ}$ that contain a subgiant (and then multiply the number identified by our empirical fraction of 9/13; see Section 3.2). We identify "MS Coll" SSGs as the products of collisions involving two main-sequence stars that occurred close enough in time to the model snapshot output time and have a product bright enough to reside in the SSG region (using the same assumptions as in Section 3.4). Finally, we identify "SG Coll" SSGs as the products of collisions involving at least one subgiant star that occurred close enough in time to the model snapshot output time. (Likely not all of these collisions would create SSGs, but this will provide an upper limit.) Through this method we identify more than 12,000 additional SSGs,[12] primarily from the "SG Mag" channel.

We plot the Poisson probabilities of observing at least one SSG from these models in bins of cluster mass within Figure 2. For the "SG MT" and "SG Mag" points, we first apply a correction factor to the number of SSGs in each model to account for a different assumed binary orbital period (or semimajor axis) distribution; we assume a log normal period distribution in Section 3, while the Monte Carlo models use a distribution that is flat in the log. For a given binary frequency, a flat distribution creates a factor of about 2.5 more short-period binaries (e.g., that can undergo RLOF on the subgiant branch) than does the log normal distribution. For all channels, we then take the average number of SSGs in each mass bin, weighted by the observed distributions of half-mass radii and cluster age (in a similar manner as described in Section 4.1). We then set t/τ from Equation (1) equal to this weighted average number of SSGs from the models in each mass bin to calculate the Poisson probabilities. The predictions from the Monte Carlo models agree well with those from our analytic upper limits from Figure 2, even given the different assumptions that go into each method. The Monte Carlo models predict a factor of a few less "MS Coll" SSGs than predicted analytically, likely due to our implicit assumptions in Section 3.4 of all encounters occurring directly at the cluster center, and with zero impact parameter (neither of which are required in the Monte Carlo model). Nonetheless, the agreement with this (relatively) independent method of deriving Ψ for all channels supports the results of our more simplified analytic calculations.

As a further step, we also investigate the grid of Monte Carlo models for predictions of the type of clusters that should harbor the most SSGs. The collision channels behave as expected, where more SSGs are produced in clusters with larger collision rates. However, the vast majority of the SSGs produced in all these Monte Carlo models (>99%) derive from the binary evolution channels. Furthermore, these models (plus our assumptions in identifying SSGs therein) predict on average about five times more "SG Mag" than "SG MT" SSGs.

We focus on these "SG MT" and "SG Mag" mechanisms here and show detailed comparisons of these two channels in Figures 5 and 6. Here we do not apply any correction to the number of SSGs from each model based on the input binary period distribution (as we did above). Some of these Monte Carlo models contain very large numbers of SSGs, inconsistent with the (much smaller) number of SSGs observed in the clusters we have studied. This likely results from a combination of initial condition choices (some of which produce clusters that do not match those we have studied) and also the details of binary evolution in BSE. However, here we are not interested in the raw number of SSGs produced; instead, we investigate trends in number of SSGs versus various cluster parameters predicted for these models.

In Figure 5, we show network diagrams to visualize how all of the parameters from a given model relate to the number of SSGs created. In this diagram, one arc around the figure corresponds to one model, hitting the axes at the appropriate values for the model, and with a color defined by the number of SSGs. In Figure 6, we plot the number of SSGs against various (mostly observable) cluster parameters.

For both channels, we see correlations of increasing number of SSGs with increasing number of stars ($N_{\rm stars}$), number of binaries ($N_{\rm b}$), and binary frequency ($f_{\rm b}$). These correlations are expected, as nearly any population of stars that involve binaries (exotic or otherwise) should behave this way. Plotting the relative number of SSGs, with respect to $N_{\rm stars}$ and $N_{\rm b}$ (second row of Figure 6), shows no significant correlation.

The more interesting result from this comparison is that the number of SSGs produced through both binary channels increases toward decreasing central density ($\log_{10}(\rho)$), increasing core radii ($r_{\rm c}$), and a decreasing ratio of the half-mass to core radii ($r_{\rm h}/r_{\rm c}$). In other words, these models predict that diffuse clusters are most efficient at producing SSGs through binary channels. Furthermore, these trends are far more dramatic for SSGs produced through ongoing mass transfer ("SG MT"). While our analytic calculations from Section 3 only account for disruptions of soft binaries, the Monte Carlo models predict that even these hard binaries can be subjected to perturbations, exchanges, etc., that can stop binaries from forming SSGs. Apparently, the mass transfer channel is particularly vulnerable to these dynamical interruptions (see also Leigh et al. 2016b).

We also investigate the relation between the number of SSGs and the core collision rate ($\Gamma_{\rm c}$; here we calculate the combined rate for 1 + 2 and 2 + 2 encounters, for a binary semimajor axis equal to the Roche radius of a 10 Gyr star at the end of the subgiant phase with a $0.45\,M_{\odot}$ MS star companion, roughly the expected mean MS mass). For both the "SG MT" and "SG Mag" channels, the number of SSGs rises toward modest $\Gamma_{\rm c}$ values ($\sim 0.03\,{\rm Myr}^{-1}$). The "SG MT" channel then decreases

[12] Collisions are tracked continuously within these models, while full snapshot output occurs roughly every 1 Gyr; common-envelope events are not tracked continuously, and therefore we cannot investigate "SG CE" here.

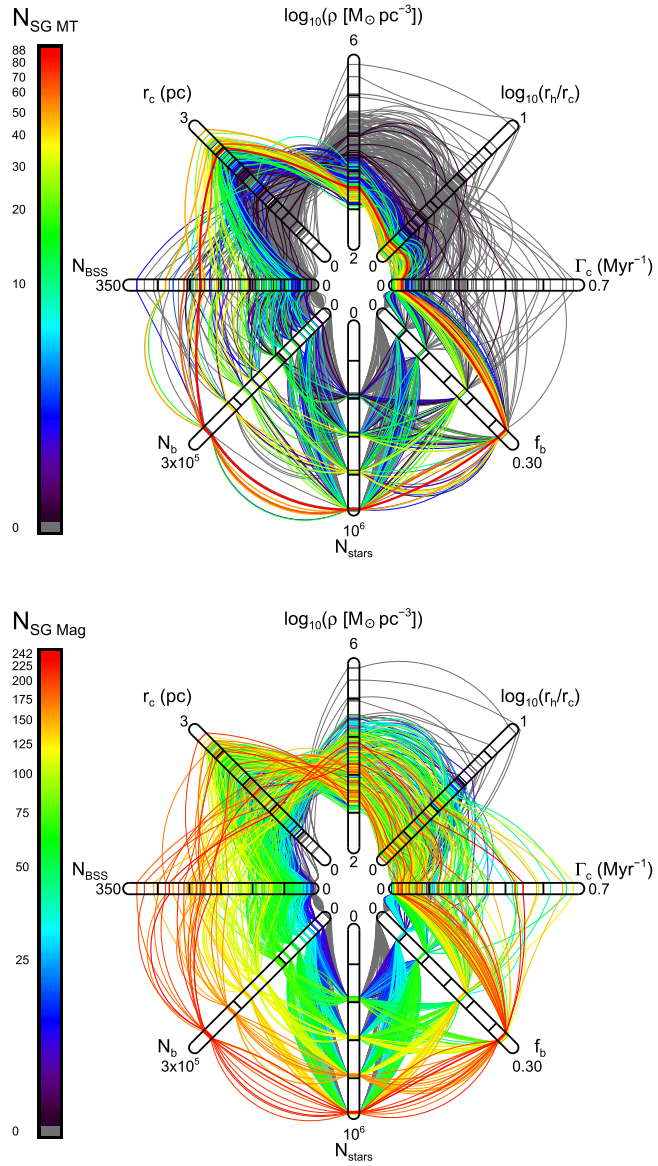

Figure 5. Comparison of the number of SSGs from the "SG MT" ($N_{\rm SG\ MT}$) and "SG Mag" ($N_{\rm SG\ Mag}$) channels, created in a grid of Monte Carlo globular cluster models that have the given total numbers of stars ($N_{\rm stars}$), binaries ($N_{\rm b}$), and BSSs ($N_{\rm BSS}$); core radius ($r_{\rm c}$); central density ($\log_{10}(\rho)$); ratio of the half-mass and core radii ($r_{\rm h}/r_{\rm c}$); core collision rate ($\Gamma_{\rm c}$); and core binary frequency ($f_{\rm b}$). These parameters are all calculated theoretically at the same snapshot times as we use to identify the SSGs, and some may be slightly different from what an observer would measure (Chatterjee et al. 2013b). We show network diagrams for each channel (top: "SG MT," bottom: "SG Mag"), where each path around the plot defines a specific cluster model, crossing the axes at the given cluster parameters, and colored by the number of SSGs created by that channel (see color bars at left of each plot).

again toward high $\Gamma_{\rm c}$ values, while the "SG Mag" channel remains roughly constant.

Generally, as $\Gamma_{\rm c}$ increases, the more frequent dynamical encounters become more efficient at hardening (i.e., shrinking the semimajor axis of) hard binaries, in this case to potentially create SSGs through both binary channels. Additionally, as $\Gamma_{\rm c}$ increases, dynamical exchanges that insert subgiants into sufficiently short-period binaries become more likely. This may account for the increase in the number of SSGs, in both binary channels, up to modest $\Gamma_{\rm c}$ values.

On the other hand, toward higher $\Gamma_{\rm c}$ values, encounters may be energetic and frequent enough to perturb binaries away from producing SSGs (e.g., through inducing binary coalescence, or otherwise inhibiting mass transfer). This may, at least partly, explain the decrease in $N_{\rm SG\ MT}$ and the flattening in $N_{\rm SG\ Mag}$ toward higher $\Gamma_{\rm c}$ values. However, we also believe that initial condition choices may contribute to this trend.

Some additional insight into this relation between $\Gamma_{\rm c}$ and the number of SSGs can be found by comparing against the number of BSSs, $N_{\rm BSS}$. BSSs are produced in the Monte Carlo model through both collisions and binary evolution, and here we include both channels in $N_{\rm BSS}$. For the few models that produce >150 BSSs (beyond the peak in the relation between $N_{\rm BSS}$ and $N_{\rm SG\ MT}$), the mean encounter rate $\langle\Gamma_{\rm c}\rangle \sim 0.19$, as compared to $\langle\Gamma_{\rm c}\rangle \sim 0.06$ for models with <150 BSSs. At the low-$N_{\rm BSS}$ and low-$\Gamma_{\rm c}$ end, both the SSGs and BSSs are produced primarily through binary evolution, and therefore the number of SSGs increases with increasing number of BSSs. However, the models with high $\Gamma_{\rm c}$ produce BSSs primarily through collisions, due to higher encounter rates. Encounters can also perturb the "proto-SG MT" binaries away from producing SSGs through mass transfer, which results in a peaked distribution of $N_{\rm BSS}$ and $N_{\rm SG\ MT}$. On the other hand, we see again that the "SG Mag" channel is less affected by dynamics, and $N_{\rm SG\ Mag}$ simply continues to increase with $N_{\rm BSS}$.

For both the "SG Mag" and "SG MT" channels, we see that the relative number of SSGs with respect to $N_{\rm BSS}$ decreases toward larger $N_{\rm BSS}$. Again, the models that produce the most BSSs do so primarily through collisions; thus, the most interesting portion of this panel is toward the low-$N_{\rm BSS}$ end, where the BSSs are produced more often through binary evolution (like the SSGs here). The models predict that for some clusters with low encounter rates, the number of SSGs may be comparable (to within a factor of a few) to the number of BSSs.

In summary, the prediction from these Monte Carlo models is that the binary evolution channels dominate the production of SSGs. Furthermore, the largest number of SSGs produced through the binary evolution channels should be found in massive, diffuse clusters with high binary frequencies and modest encounter rates. At present, the observed data are too sparse to search for a trend in number of SSGs with encounter rate. Nonetheless, this result from the Monte Carlo models aligns with our suggestion in Paper I that dynamical disruptions, perturbations, and other alterations to "proto-SSG" binaries could explain the empirical trend of decreasing specific SSG frequency with increasing cluster mass (Figure 4). These dynamical effects inhibit the binary evolution channels, and particularly the "SG MT" channel, in clusters with higher encounter rates (like those in our observed sample of globular clusters). Clusters with the highest encounter rates may begin to produce SSGs through the collision mechanisms at a similar, or perhaps higher, rate than the binary mechanisms.

6. Discussion and Conclusions

In Paper I, we identify from the literature a sample of 65 SSG and RS stars in 16 star clusters, including both open and globular clusters, and we summarize their empirical demographics within this paper in Section 1. In Paper II, we discuss in detail three potential formation channels for SSGs. The mechanisms within these channels involve isolated subgiant binary evolution, rapid partial stripping of a subgiant's

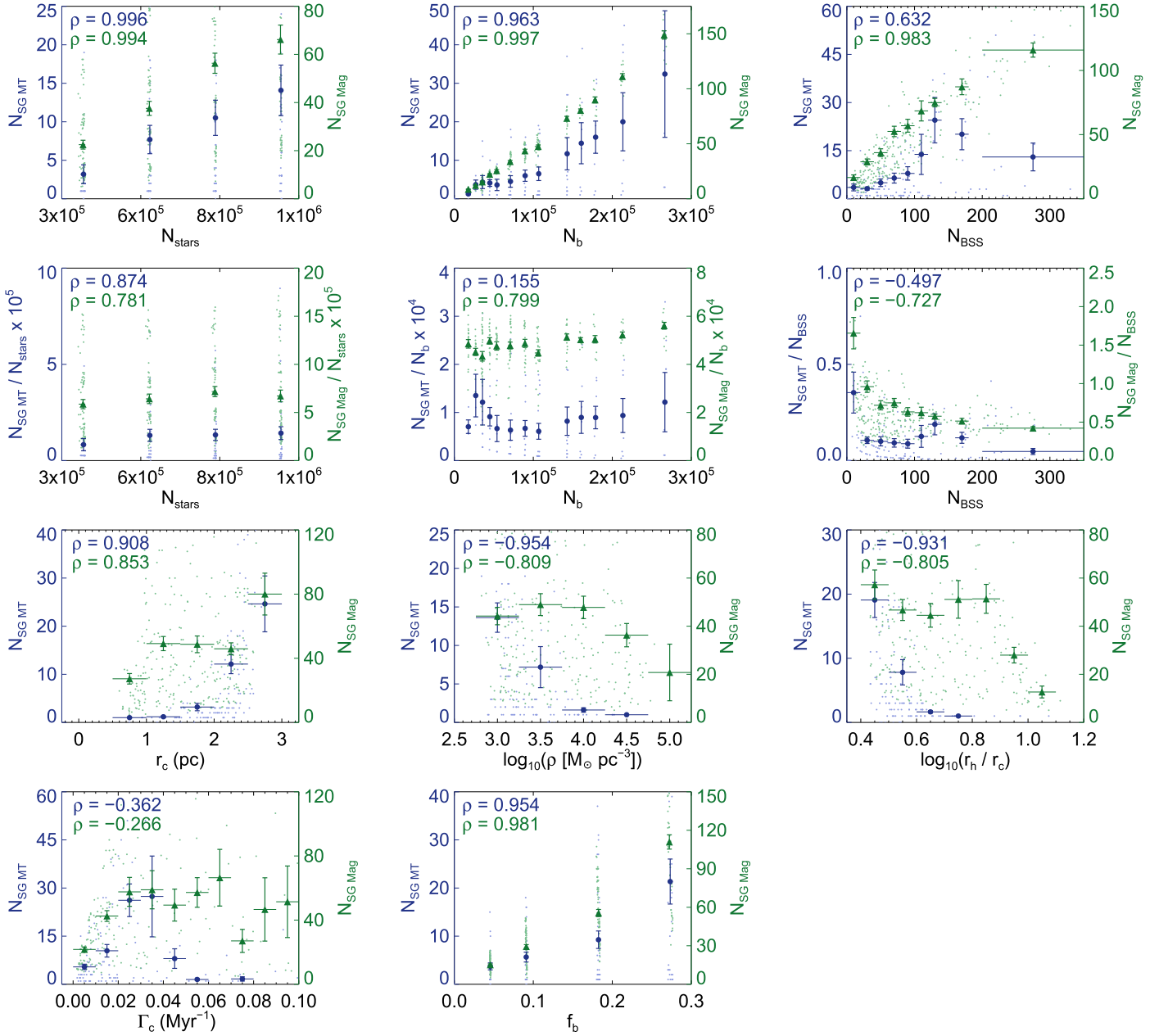

Figure 6. Comparison of the number of SSGs from the "SG MT" ($N_{\rm SG\ MT}$; blue circles) and "SG Mag" ($N_{\rm SG\ Mag}$; green triangles) channels, created in a grid of Monte Carlo globular cluster models and showing the same parameters as in Figure 5. Here we plot the number of SSGs as a function of each of these parameters respectively, showing only models that produced at least one SSG. Small points show the raw values from the grid, and larger points show the mean values in bins, with vertical error bars equal to the standard errors of the mean and horizontal lines showing the bin sizes (which are smaller than the symbols in some cases). For reference, we also include the respective Pearson correlation statistics (ρ), calculated for the mean values, in each panel.

envelope (for which we envision two mechanisms, one through common-envelope evolution and another through dynamical encounters), or reduced luminosity due to magnetic fields that inhibit convection. In addition, Paper II briefly considers a formation channel through collisions of two main-sequence stars during a binary encounter, which we elaborate on here.

With isolated binaries, SSGs may be produced through ongoing binary mass transfer involving a subgiant star (Section 2.1, "SG MT"), reduced convective efficiency on a rapidly rotating magnetically active subgiant, likely in a tidally locked binary (Section 2.2, "SG Mag"), or rapid stripping of a subgiant's envelope during a common-envelope phase (Section 2.3, "SG CE"). Invoking stellar collisions (most likely involving at least one binary; Leigh & Geller 2012, 2013), SSGs can be created through the collision and subsequent merger of two MS stars observed while contracting back onto the MS (Section 2.4, "MS Coll"), or a grazing collision involving a subgiant that rapidly strips much of its envelope (Section 2.3, "SG Coll"). The binary evolution channels can happen in isolation, while the collision channels require the dynamical environment of a star cluster (or perhaps gravitational perturbations from a more distant companion star). Yet all of these channels are catalyzed by binary stars.

Our analytic Poisson probability calculations (Sections 3 and 4, which are upper limits) and our analysis of a large grid of Monte Carlo models (Section 5) suggest that the binary evolution channels are dominant. In particular, both of these methods predict that we are most likely to observe SSGs that

originate from magnetically active subgiants with reduced convective efficiency (see Figures 2 and 3).

This result is based on the SSG formation rates alone, without any constraint on the expected binarity of the product. Observationally, we know that the SSGs are primarily in short-period active binaries (Paper I; see also Section 1 here). At least two-thirds of the SSGs have photometric and/or radial velocity periods of $\lesssim$15 days, and at least three-quarters of these variables are confirmed to be radial velocity binaries. These short orbital periods are consistent with tidally locked binaries (e.g., Meibom & Mathieu 2005), as expected for the "SG Mag" mechanism. The SSGs with the shortest-period variability may be in binaries currently (or very recently) undergoing mass transfer. Indeed, there are a few W UMa contact binaries among the SSGs in our sample (in NGC 188, ω Centauri, and NGC 6397), which support the "SG MT" mechanism. In short, the "SG MT" and "SG Mag" mechanisms naturally explain the binarity.

Additional empirical evidence supporting SSG formation through isolated binary evolution may be found in the nearly 10,000 stars in the "No-Man's-Land" from *Kepler* (Batalha et al. 2013; Huber et al. 2014), which may be field SSGs. These stars are important targets for future observations, and we will investigate them in more detail within a future paper.

Conversely, producing SSGs through collisions may only be relevant in very dense star clusters. Furthermore, encounters that lead to the "MS Coll" mechanism generally produce collision products in wider binaries (or without companions), sometimes with periods that are orders of magnitude larger than observed for the SSGs (Leigh et al. 2011; Geller et al. 2013). When also considering the low Poisson probabilities calculated here for the "MS Coll" channel, and the even lower number predicted by the Monte Carlo models (see Figure 2 and Section 5), we conclude that, in most clusters, observing an SSG from the "MS Coll" channel is unlikely, especially for an SSG found in a short-period binary. The few globular clusters studied in Paper I with very high encounter rates may be the best places to find SSGs produced through this mechanism (see Section 4.2 and Table 1).

Observing an SSG resulting from the rapid loss of a subgiant's envelope ("SG Strip"), through either mechanism explored here, is also relatively unlikely, given our Poisson probability calculations and our analysis of the Monte Carlo models. The expected binarity of the product for "SG Strip" is less clear than for the other mechanisms. It may be possible that a grazing encounter that strips a subgiant's envelope can leave a bound companion in a short-period binary (akin to a tidal capture binary), but further study is required to confirm whether this is indeed possible. Likewise stripping in common-envelope evolution is highly uncertain, and it is unclear what the binarity of the product would be.

Other efficient mechanisms may also exist that we have not identified, which could explain why our $\Psi(n_{\rm SSG})$ Poisson probabilities do not reach unity for some clusters (and particularly the open clusters) in Table 1, where $n_{\rm SSG}$ SSGs are in fact observed. For instance, there may be other "SG Strip" mechanisms that we have not investigated. Perhaps SSGs can be created if stable mass transfer is interrupted dynamically, as discussed in Leigh et al. (2016b). In addition, very close companions to neutron stars can be evaporated, as in the well-known "black widow" pulsars (e.g., Fruchter et al. 1990). Perhaps companions in the early stages of being evaporated would appear as SSGs, as may be the case for SSG U12 in NGC 6397 (D'Amico et al. 2001; Ferraro et al. 2003).

Massive and diffuse globular clusters may be the most promising targets for future observations aimed at identifying additional SSGs. The Monte Carlo globular cluster models (Section 5) predict that such clusters should have the largest frequency of SSGs created through the binary evolution channels. The Monte Carlo models also predict that the binary evolution channels may be inhibited for the densest clusters with high encounter rates, which is consistent with the current observations (Figure 4, though note that the observations are incomplete; see Paper I). It is clear that in some clusters multiple mechanisms likely operate simultaneously to produce SSGs (see, e.g., Table 1).

Many of these observed and predicted trends in number of SSGs are also seen for BSSs. For instance, the frequency of BSSs in globular clusters is observed to be anticorrelated with the absolute luminosity (mass) of the cluster (Piotto et al. 2004; Leigh et al. 2007), but correlated with the binary fraction (Sollima et al. 2008; Milone et al. 2012). These observations point to binaries as a critical ingredient for BSS formation in globular clusters (Knigge et al. 2009). The correlations seen in globular cluster observations have been interpreted theoretically to indicate that binary evolution is an important, and sometimes dominant, BSS production mechanism (Leigh et al. 2011), though binary-mediated collisions may also be important at high densities (Chatterjee et al. 2013a; Sills et al. 2013). The reduced survival of binaries (i.e., BSS and SSG progenitors) in high-density (and high-velocity-dispersion) environments likely also contributes to these observed correlations (Davies et al. 2004; Sollima 2008), as does the preferential retention of binary stars, compared to the less massive single stars, in clusters that experience significant mass loss (as may be the case for the lower-mass clusters in our observed SSG sample). Binaries are also critical for BSS (and likely also SSG) formation in open clusters (Mathieu & Geller 2009) and the field (Carney et al. 2005). The discussion from this body of literature may help to explain the observed decreasing trend in specific frequency of SSGs with increasing cluster mass, shown in Figure 4.

Though we focus on the SSGs throughout the majority of the paper, the RS stars (i.e., stars that occupy the lighter-gray regions in Figure 1) have very similar empirical characteristics (Paper I). As shown in Figure 1, RS and SSG stars may be produced through the same mechanisms, and in some cases one can be the evolutionary precursor to the other. Furthermore, at least two of these mechanisms that form SSGs, mass transfer and MS–MS collisions, are also invoked to explain the origins of BSSs and yellow stragglers/giants (McCrea 1964; Mathieu & Latham 1986; Leonard 1989; Chen & Han 2008; Leigh et al. 2011; Chatterjee et al. 2013a; Sills et al. 2013; Gosnell et al. 2015; Leiner et al. 2016). Some fraction of these stars may have been born through the same (or similar) formation channels, and perhaps in some cases these stars may represent different stages along the same evolutionary sequence. Comparing the frequencies and binary characteristics of these stellar populations across multiple star clusters could reveal important insights into their formation mechanism(s) and provide important guidance for detailed evolutionary models of binary mass transfer and the products of stellar collisions.

A.M.G. acknowledges support from NASA through *HST* grant AR-13910 and a National Science Foundation Astronomy and Astrophysics Postdoctoral Fellowship Award No. AST-1302765. S.C. acknowledges support from NASA through *HST* grant *HST*-AR-12829.004-A. Support for Programs AR-13910 and *HST*-AR-12829.004-A was provided by NASA through a grant from the Space Telescope Science Institute, which is operated by the Association of Universities for Research in Astronomy, Inc., under NASA contract NAS5-26555. This research was supported in part through the computational resources and staff contributions provided for the Quest high-performance computing facility at Northwestern University, which is jointly supported by the Office of the Provost, the Office for Research, and Northwestern University Information Technology.

References

Aarseth, S. J. 1999, PASP, 111, 1333
Alexander, P. E. R., & Gieles, M. 2012, MNRAS, 422, 3415
Alexander, P. E. R., Gieles, M., Lamers, H. J. G. L. M., & Baumgardt, H. 2014, MNRAS, 442, 1265
Batalha, N. M., Rowe, J. F., Bryson, S. T., et al. 2013, ApJS, 204, 24
Belczynski, K., Kalogera, V., Rasio, F. A., et al. 2008, ApJS, 174, 223
Bressan, A., Marigo, P., Girardi, L., et al. 2012, MNRAS, 427, 127
Carney, B. W., Lee, J.-W., & Dodson, B. 2005, AJ, 129, 656
Carraro, G., Girardi, L., & Marigo, P. 2002, MNRAS, 332, 705
Chabrier, G., Gallardo, J., & Baraffe, I. 2007, A&A, 472, L17
Chatterjee, S., Fregeau, J. M., Umbreit, S., & Rasio, F. A. 2010, ApJ, 719, 915
Chatterjee, S., Rasio, F. A., Sills, A., & Glebbeek, E. 2013a, ApJ, 777, 106
Chatterjee, S., Umbreit, S., Fregeau, J. M., & Rasio, F. A. 2013b, MNRAS, 429, 2881
Chen, X., & Han, Z. 2008, MNRAS, 387, 1416
Chumak, Y. O., Platais, I., McLaughlin, D. E., Rastorguev, A. S., & Chumak, O. V. 2010, MNRAS, 402, 1841
Clausen, J. V., Bruntt, H., Claret, A., et al. 2009, A&A, 502, 253
D'Amico, N., Possenti, A., Manchester, R. N., et al. 2001, ApJL, 561, L89
Davies, M. B., Piotto, G., & de Angeli, F. 2004, MNRAS, 349, 129
Di Cecco, A., Bono, G., Prada Moroni, P. G., et al. 2015, AJ, 150, 51
Eggleton, P. 2006, Evolutionary Processes in Binary and Multiple Stars (Cambridge: Cambridge Univ. Press)
Eggleton, P. P. 1983, ApJ, 268, 368
Fabian, A. C., Pringle, J. E., & Rees, M. J. 1975, MNRAS, 172, 15P
Ferraro, F. R., Sabbi, E., Gratton, R., et al. 2003, ApJL, 584, L13
Fregeau, J. M., Cheung, P., Portegies Zwart, S. F., & Rasio, F. A. 2004, MNRAS, 352, 1
Fregeau, J. M., Gürkan, M. A., Joshi, K. J., & Rasio, F. A. 2003, ApJ, 593, 772
Fregeau, J. M., & Rasio, F. A. 2007, ApJ, 658, 1047
Fruchter, A. S., Berman, G., Bower, G., et al. 1990, ApJ, 351, 642
Geller, A. M., Hurley, J. R., & Mathieu, R. D. 2013, AJ, 145, 8
Geller, A. M., Latham, D. W., & Mathieu, R. D. 2015, AJ, 150, 97
Geller, A. M., & Leigh, N. W. C. 2015, ApJL, 808, L25
Geller, A. M., Leiner, E. M., Bellini, A., et al. 2017, ApJ, 840, 66
Geller, A. M., & Mathieu, R. D. 2011, Natur, 478, 356
Geller, A. M., & Mathieu, R. D. 2012, AJ, 144, 54
Geller, A. M., Mathieu, R. D., Harris, H. C., & McClure, R. D. 2008, AJ, 135, 2264
Gieles, M., Alexander, P. E. R., Lamers, H. J. G. L. M., & Baumgardt, H. 2014, MNRAS, 437, 916
Gosnell, N. M., Mathieu, R. D., Geller, A. M., et al. 2015, ApJ, 814, 163
Harris, W. E. 1996, AJ, 112, 1487
Harris, W. E. 2010, arXiv:1012.3224
Hills, J. G., & Day, C. A. 1976, ApL, 17, 87
Hole, K. T., Geller, A. M., Mathieu, R. D., et al. 2009, AJ, 138, 159
Huber, D., Silva Aguirre, V., Matthews, J. M., et al. 2014, ApJS, 211, 2
Hurley, J. R., Pols, O. R., Aarseth, S. J., & Tout, C. A. 2005, MNRAS, 363, 293
Hurley, J. R., Pols, O. R., & Tout, C. A. 2000, MNRAS, 315, 543
Hurley, J. R., Tout, C. A., & Pols, O. R. 2002, MNRAS, 329, 897
Joshi, K. J., Nave, C. P., & Rasio, F. A. 2001, ApJ, 550, 691
Joshi, K. J., Rasio, F. A., & Portegies Zwart, S. 2000, ApJ, 540, 969
Kalirai, J. S., Richer, H. B., Fahlman, G. G., et al. 2001, AJ, 122, 266
Kharchenko, N. V., Piskunov, A. E., Schilbach, E., Röser, S., & Scholz, R.-D. 2013, A&A, 558, A53
Knigge, C., Leigh, N., & Sills, A. 2009, Natur, 457, 288
Kroupa, P. 2001, MNRAS, 322, 231
Leigh, N., & Geller, A. M. 2012, MNRAS, 425, 2369
Leigh, N., Knigge, C., Sills, A., et al. 2013, MNRAS, 428, 897
Leigh, N., & Sills, A. 2011, MNRAS, 410, 2370
Leigh, N., Sills, A., & Knigge, C. 2007, ApJ, 661, 210
Leigh, N., Sills, A., & Knigge, C. 2011, MNRAS, 416, 1410
Leigh, N. W. C., Antonini, F., Stone, N. C., Shara, M. M., & Merritt, D. 2016a, MNRAS, 463, 1605
Leigh, N. W. C., & Geller, A. M. 2013, MNRAS, 432, 2474
Leigh, N. W. C., Geller, A. M., & Toonen, S. 2016b, ApJ, 818, 21
Leiner, E., Mathieu, R. D., & Geller, A. M. 2017, ApJ, 840, 67
Leiner, E., Mathieu, R. D., Stello, D., Vanderburg, A., & Sandquist, E. 2016, ApJL, 832, L13
Leonard, P. J. T. 1989, AJ, 98, 217
Marín-Franch, A., Aparicio, A., Piotto, G., et al. 2009, ApJ, 694, 1498
Mathieu, R. D., & Geller, A. M. 2009, Natur, 462, 1032
Mathieu, R. D., & Latham, D. W. 1986, AJ, 92, 1364
McCrea, W. H. 1964, MNRAS, 128, 147
Meibom, S., Grundahl, F., Clausen, J. V., et al. 2009, AJ, 137, 5086
Meibom, S., & Mathieu, R. D. 2005, ApJ, 620, 970
Milliman, K. E., Mathieu, R. D., Geller, A. M., et al. 2014, AJ, 148, 38
Milone, A. P., Piotto, G., Bedin, L. R., et al. 2012, A&A, 540, A16
Paxton, B., Marchant, P., Schwab, J., et al. 2015, ApJS, 220, 15
Piotto, G., De Angeli, F., King, I. R., et al. 2004, ApJL, 604, L109
Piskunov, A. E., Schilbach, E., Kharchenko, N. V., Röser, S., & Scholz, R.-D. 2008, A&A, 477, 165
Platais, I., Cudworth, K. M., Kozhurina-Platais, V., et al. 2011, ApJL, 733, L1
Plummer, H. C. 1911, MNRAS, 71, 460
Press, W. H., & Teukolsky, S. A. 1977, ApJ, 213, 183
Raghavan, D., McAlister, H. A., Henry, T. J., et al. 2010, ApJS, 190, 1
Salaris, M., Weiss, A., & Percival, S. M. 2004, A&A, 414, 163
Sandquist, E. L., Shetrone, M., Serio, A. W., & Orosz, J. 2013, AJ, 146, 40
Sarajedini, A., von Hippel, T., Kozhurina-Platais, V., & Demarque, P. 1999, AJ, 118, 2894
Sills, A., Adams, T., & Davies, M. B. 2005, MNRAS, 358, 716
Sills, A., Adams, T., Davies, M. B., & Bate, M. R. 2002, MNRAS, 332, 49
Sills, A., Faber, J. A., Lombardi, J. C., Jr., Rasio, F. A., & Warren, A. R. 2001, ApJ, 548, 323
Sills, A., Glebbeek, E., Chatterjee, S., & Rasio, F. A. 2013, ApJ, 777, 105
Sills, A., Karakas, A., & Lattanzio, J. 2009, ApJ, 692, 1411
Sills, A., Lombardi, J. C., Jr., Bailyn, C. D., et al. 1997, ApJ, 487, 290
Sollima, A. 2008, MNRAS, 388, 307
Sollima, A., Lanzoni, B., Beccari, G., Ferraro, F. R., & Fusi Pecci, F. 2008, A&A, 481, 701
Straižys, V., Maskoliūnas, M., Boyle, R. P., et al. 2014, MNRAS, 437, 1628
Thompson, I. B., Kaluzny, J., Rucinski, S. M., et al. 2010, AJ, 139, 329
Tian, B., Deng, L., Han, Z., & Zhang, X. B. 2006, A&A, 455, 247
Tofflemire, B. M., Gosnell, N. M., Mathieu, R. D., & Platais, I. 2014, AJ, 148, 61
Umbreit, S., Fregeau, J. M., Chatterjee, S., & Rasio, F. A. 2012, ApJ, 750, 31
van den Bergh, S. 2006, AJ, 131, 1559
Webb, J. J., & Leigh, N. W. C. 2015, MNRAS, 453, 3278